International Journal of Energetica (IJECA)
https://www.ijeca.info
ISSN: 2543-3717 Volume 10. Issue 2. 2025
Page 74-85

Effect of Microchannel Aspect Ratio on Laminar Nanofluid Flow and Thermal Performance: A Three-Dimensional Numerical Study

Saleh Etaig[1*], Nabil Elsharif[1]

[1]*Mechanical engineering Department, Faculty of Engineering Department, University of Benghazi, Benghazi, LIBYA*

*Corresponding author E-mail: *Saleh.Etaig@uob.edu.ly*

Abstract –*Microchannel heat sinks have emerged as an effective thermal management solution for compact electronic and energy systems subjected to high heat fluxes. In parallel, nanofluids have been proposed as advanced working fluids capable of enhancing convective heat transfer due to their improved thermophysical properties. In this study, a three-dimensional numerical investigation of laminar nanofluid flow and heat transfer in rectangular microchannels is conducted with a focus on the combined effects of geometric and operating parameters. An Al_2O_3–water nanofluid is employed as the working fluid and modeled as a homogeneous single-phase Newtonian fluid. The governing equations of mass, momentum, and energy conservation are solved using the finite volume method under steady-state conditions. Uniform heat flux is applied to three channel walls, while the remaining wall is assumed adiabatic. The influence of microchannel aspect ratio, hydraulic diameter, and Reynolds number on velocity distribution, temperature fields, and Nusselt number is systematically examined. The results indicate that Reynolds number is the dominant parameter controlling convective heat transfer enhancement, while increasing hydraulic diameter and aspect ratio generally reduce thermal performance under laminar conditions. The findings provide design-oriented insights for efficient rectangular microchannel heat sinks employing nanofluids in advanced thermal management applications.*

Keywords: *Microchannel heat sink, Nanofluid, Numerical investigation, Convective heat transfer, Laminar flow*

Received: 20/10/2025 – Revised: 03/11/2025 – Accepted: 25/12/2025

I. Introduction

Microchannel heat sinks were first introduced as an effective solution for high heat-flux cooling in microelectronic devices and have since become a central topic in microscale heat transfer research [1–9]. Early experimental and numerical investigations established the fundamental characteristics of single-phase flow and heat transfer in microchannels and microtubes, highlighting deviations from classical macroscale correlations [10–18].

Rectangular and non-circular microchannels have received extensive attention due to their relevance to silicon-based fabrication and practical heat sink design. Numerous studies have shown that channel geometry, surface condition, and aspect ratio significantly influence pressure drop, velocity distribution, and heat transfer performance [19–31]. Bias effects, measurement uncertainty, and surface roughness have also been reported to affect experimental heat transfer data in microchannel flows [32–36].

In parallel with geometric optimization, nanofluids have emerged as advanced working fluids for enhancing convective heat transfer. Experimental and numerical investigations demonstrated improved thermal performance of nanofluids in microchannels, microtubes, and confined cooling systems compared with conventional base fluids [37–41]. Comprehensive

reviews summarized the mechanisms, advantages, and limitations of nanofluid heat transfer in porous media and microscale applications [42].

Accurate prediction of nanofluid flow and heat transfer requires reliable modeling of thermophysical properties and transport mechanisms. Several studies proposed effective viscosity models and investigated the influence of Brownian motion and near-wall particle dynamics on nanofluid behavior under laminar and natural convection conditions [43–48].

Beyond microchannel heat sinks, nanofluids have been successfully applied to a wide range of energy systems, including shell-and-tube heat exchangers and photovoltaic/thermal (PV/T) systems, where enhanced coolant performance improves heat removal and overall energy efficiency [49–45]. Despite these advances, comprehensive three-dimensional numerical studies that simultaneously examine the combined effects of aspect ratio, hydraulic diameter, and Reynolds number on nanofluid heat transfer in rectangular microchannels remain limited.

The novelty of this study lies in providing a systematic three-dimensional numerical assessment of laminar nanofluid flow and heat transfer in rectangular microchannels with explicit emphasis on aspect-ratio variation under uniform wall heat flux conditions. Unlike many previous studies that focus on a single geometric configuration or report isolated trends, the present work simultaneously examines the coupled effects of aspect ratio, hydraulic diameter, and Reynolds number within a unified numerical framework. In addition, the study offers a balanced thermal–hydraulic evaluation by quantifying both heat transfer enhancement and pressure drop penalties, thereby enabling meaningful performance trade-off analysis. This integrated approach provides design-oriented insight that supports the optimized selection of rectangular microchannel geometries for nanofluid-based cooling applications.

II. Numerical Methodology

2.1. Physical Model and Geometry

A three-dimensional rectangular microchannel is considered in the present numerical investigation. The microchannel has a fixed length of 25 mm, while the cross-sectional geometry is varied to examine the influence of aspect ratio and hydraulic diameter on flow and heat transfer characteristics. Several channel configurations are analyzed, with aspect ratios ranging from 1.0 to 4.5 and hydraulic diameters between 350 μm and 850 μm. These ranges are selected to represent typical geometries used in compact microchannel heat sinks for electronic and energy system cooling applications. Figure 1 shows the geometry domain.

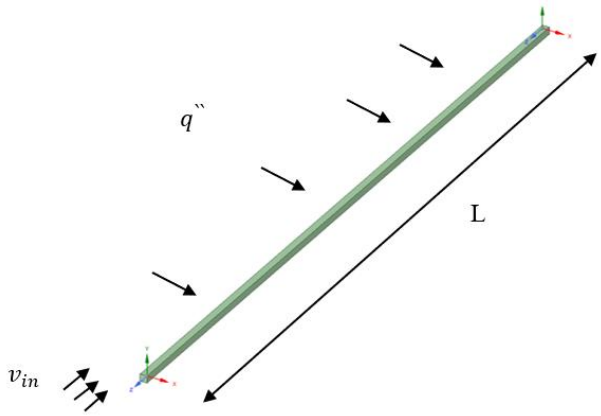

Figure 1. Geometry Domain

The computational domain consists of a single straight microchannel, assuming uniform cross-sectional geometry along the flow direction. The nanofluid enters the channel through a fully developed velocity profile at the inlet and exits at the outlet under constant pressure conditions. Three channel walls are subjected to a uniform heat flux, while the remaining wall is assumed to be adiabatic, representing typical asymmetric heating conditions encountered in practical microchannel heat sink designs. Table 1 outlines the geometric dimensions for each simulation case. It specifies the variations in aspect ratios and hydraulic diameters used to evaluate their influence on the microchannel's thermal performance.

Table 1. Microchannel dimensions used for numerical simulations for each case with Varity aspect ratios and hydraulic diameters

D_h (μm)	AS (a/b)	a(μm)	b(μm)	l (mm)	D_h (μm)	AS (a/b)	a(μm)	b (μm)	l (mm)
350	1	350	350	25	450	1	450	450	25
	1.75	275	481.25	25		1.75	353.57	618.75	25
	2.5	245	612.5	25		2.5	315	787.5	25
	3.5	225	787.5	25		3.5	289.29	1012.5	25
	4.5	213.89	962.5	25		4.5	275	1237.5	25
600	1	600	600	25	850	1	850	850	25
	1.75	471.43	825	25		1.75	667.86	1168.75	25
	2.5	420	1050	25		2.5	595	1487.5	25
	3.5	385.71	1350	25		3.5	456.42	1912.5	25
	4.5	366.66	1650	25		4.5	519.44	2337.5	25

2.2. Governing Equations

The flow is assumed to be steady, laminar, incompressible, and three-dimensional. The nanofluid is modeled as a homogeneous single-phase Newtonian fluid, an assumption widely adopted for low nanoparticle volume fractions and laminar flow regimes. Under these

assumptions, the governing equations consist of the continuity, momentum, and energy equations, expressed as:

Continuity equation

$$\frac{\partial \rho}{\partial t} + \frac{\partial}{\partial x}(\rho u) + \frac{\partial}{\partial y}(\rho v) + \frac{\partial}{\partial z}(\rho w) = 0 \quad (1)$$

Momentum equations

$$\rho g_x - \frac{\partial p}{\partial x} + \frac{\partial \tau_{xx}}{\partial x} + \frac{\partial \tau_{yx}}{\partial y} + \frac{\partial \tau_{zx}}{\partial z} = \rho\left(\frac{\partial u}{\partial t} + u\frac{\partial u}{\partial x} + v\frac{\partial u}{\partial y} + w\frac{\partial u}{\partial z}\right) \quad (2)$$

$$\rho g_y - \frac{\partial p}{\partial y} + \frac{\partial \tau_{xy}}{\partial x} + \frac{\partial \tau_{yy}}{\partial y} + \frac{\partial \tau_{zy}}{\partial z} = \rho\left(\frac{\partial v}{\partial t} + u\frac{\partial v}{\partial x} + v\frac{\partial v}{\partial y} + w\frac{\partial v}{\partial z}\right) \quad (3)$$

$$\rho g_z - \frac{\partial p}{\partial z} + \frac{\partial \tau_{xz}}{\partial x} + \frac{\partial \tau_{yz}}{\partial y} + \frac{\partial \tau_{zz}}{\partial z} = \rho\left(\frac{\partial w}{\partial t} + u\frac{\partial w}{\partial x} + v\frac{\partial w}{\partial y} + w\frac{\partial w}{\partial z}\right) \quad (4)$$

Energy equation

$$\rho \frac{d\hat{u}}{dt} + p(\nabla \cdot V) = \nabla \cdot (k\nabla T) + \Phi \quad (5)$$

2.3. Thermophysical Properties of the Nanofluid

$$\mu nf = \mu f(1-\emptyset)2.5 \quad (6)$$

$$\rho nf = 1 - \emptyset\rho f + \emptyset\rho s \quad (7)$$

$$(\rho Cp)nf = (1-\emptyset)(\rho Cp)f + \emptyset(\rho Cp)s \quad (8)$$

$$\frac{k_{nf}}{k_f} = \frac{(k_s + 2k_f) - 2\emptyset(k_f - k_s)}{(k_s + 2k_f) - \emptyset(k_f - k_s)} \quad (9)$$

Table 2 summarizes the thermophysical properties of water and Al_2O_3 nanoparticles used in this study. These values are essential for calculating the effective properties of the nanofluid mixture during the simulation

Table 2. Thermophysical Properties of Water and Nanoparticles

Physical Properties	Pure Water	Al_2O_3
C_p (J/kg k)	4179	765
ρ (kg/m^3)	997.1	3970
k (W/m k)	0.613	40
μ(N.s/m^2)	0.000855	-

2.4. Boundary Conditions

At the microchannel inlet, a uniform velocity profile corresponding to the desired Reynolds number is imposed, along with a constant inlet temperature. The Reynolds number is defined based on the hydraulic diameter and nanofluid properties and is varied to investigate its influence on flow and heat transfer behavior.

At the outlet, a zero-gauge pressure condition is applied, allowing the flow to exit the computational domain freely. No-slip velocity boundary conditions are imposed on all channel walls. A constant heat flux is applied on three walls, while the fourth wall is treated as adiabatic. Heat conduction within the channel walls is neglected, and radiation effects are assumed to be insignificant due to the microscale dimensions and moderate operating temperatures.

2.5. Numerical Solution Procedure

The governing equations are solved using the finite volume method implemented in a commercial CFD solver. Pressure–velocity coupling is handled using the SIMPLE algorithm. Second-order upwind discretization schemes are employed for the convective terms in the momentum and energy equations to enhance solution accuracy.

Convergence is achieved when the residuals of continuity, momentum, and energy equations fall below 10−6, and additional monitoring of key parameters such as outlet temperature and pressure drop confirms solution stability. Grid independence studies are performed to ensure that numerical results are independent of mesh resolution, and the final mesh is selected based on a compromise between accuracy and computational cost.

2.6. Post-Processing and Data Reduction

The local and average Nusselt numbers are calculated based on the applied heat flux, wall temperature, and bulk fluid temperature. The bulk temperature is evaluated using a mass-weighted average over the channel cross-section. Pressure drop across the microchannel is obtained from the difference between inlet and outlet pressures. These parameters are used to assess the combined effects of Reynolds number, aspect ratio, and hydraulic diameter on the thermal and hydraulic performance of the microchannel.

2.7. Model Validation

To ensure the accuracy and reliability of the numerical model, validation was performed by comparing the present simulation results with well-established experimental and numerical data available in the literature for laminar single-phase flow and heat transfer in rectangular microchannels. Validation focused on key dimensionless parameters, including the Nusselt number and friction factor, which are commonly used to assess

thermal and hydraulic performance in microscale channels.

As shown in Figure 2, simulations were conducted for water flow in rectangular microchannels under identical geometric configurations and operating conditions reported in previous experimental studies. The predicted average Nusselt numbers were compared with classical correlations and experimental data for laminar flow in microchannels. Good agreement was observed, with deviations generally within ±5–8%, which is consistent with discrepancies reported in similar numerical investigations and can be attributed to differences in boundary conditions, entrance effects, and thermophysical property assumptions.

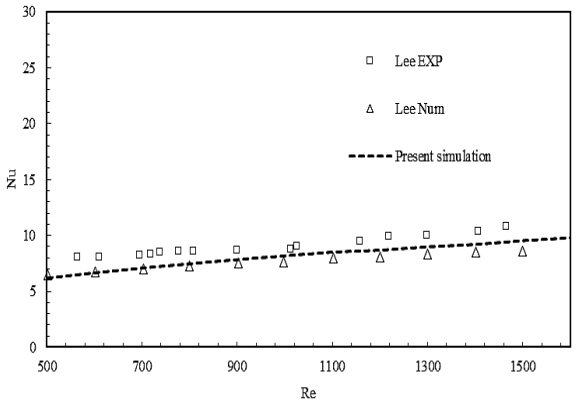

Figure 2. Results validations with Lee experiment[44]

In addition, the numerical predictions of pressure drop and friction factor were compared with published experimental measurements for laminar flow in rectangular microchannels over comparable Reynolds number ranges. The predicted trends closely followed the reference data, confirming the model's ability to accurately capture viscous effects and momentum transport in confined geometries.

For nanofluid validation, the present numerical results were compared with reported numerical and experimental studies on Al_2O_3–water nanofluid flow in microchannels. The predicted enhancement in Nusselt number with increasing Reynolds number and nanoparticle concentration showed good qualitative and quantitative agreement with the literature. Minor discrepancies were observed at higher Reynolds numbers, which can be attributed to differences in nanofluid property models and assumptions regarding nanoparticle–fluid interactions. Overall, the validation results demonstrate that the present numerical model is capable of reliably predicting laminar flow behavior, heat transfer characteristics, and pressure drop in rectangular microchannels using nanofluids. This provides confidence in the applicability of the model for the parametric investigations presented in this study. "The validation of the local Nusselt number along the channel wall against the results of Salman et al. [45] is illustrated in Figure 3, showing a strong agreement between the present numerical model and the reference data."

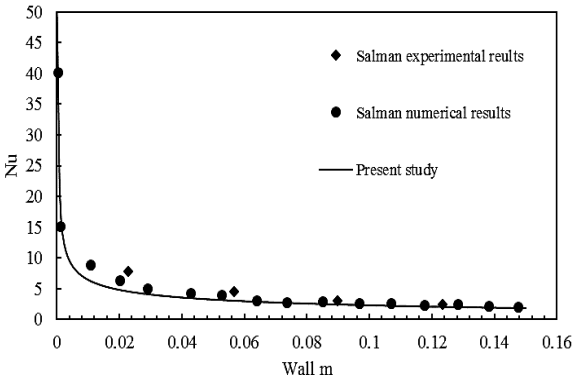

Figure 3. Results validations with Salman et al[45]

III. Results and Discussion

3.1. Effect of Re number and Flow Development

Figure 4 illustrates the local temperature contours at the mid-plane of the microchannel for different Reynolds numbers and aspect ratios. As expected, the maximum temperature is located at the upper two corners with increasing Reynolds number, in all cross sections, a low-temperature region (blue) dominates the channel core, while higher temperatures (yellow–red) appear near the channel walls. This behavior is characteristic of laminar flow in microchannels, where heat is primarily transferred by conduction in the transverse direction and by convection along the flow direction.

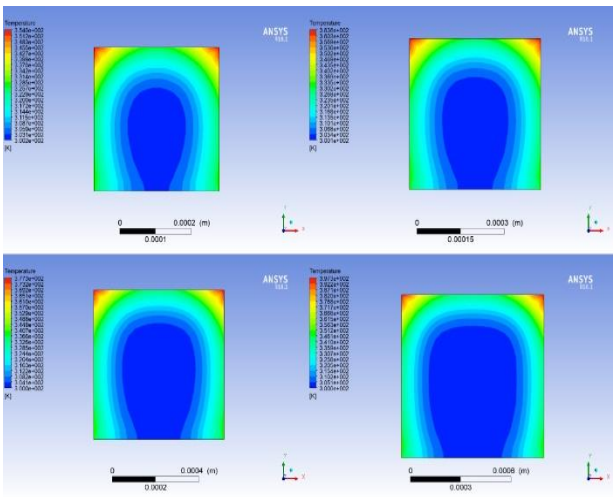

Figure 4. Local temperature on middle plane of microchannels with (AR=1, Dh = 350, 450, 600, 850 μm, Re =300)

The influence of aspect ratio on velocity distribution is clearly observed in Figure 4. For higher aspect ratios, the velocity gradients near the longer walls become more pronounced, leading to non-uniform shear stress distribution along the perimeter. This redistribution of velocity plays an important role in shaping the thermal boundary layer development and, consequently, the heat transfer behavior.

Figure 5 presents the local temperature contours at the middle plane of square microchannels (AR=1) for different hydraulic diameters (Dh) at a fixed Reynolds number of 800. These results clearly demonstrate the influence of channel size on thermal behavior under identical flow conditions; a clear trend is observed as the hydraulic diameter increases from 350 µm to 850 µm.

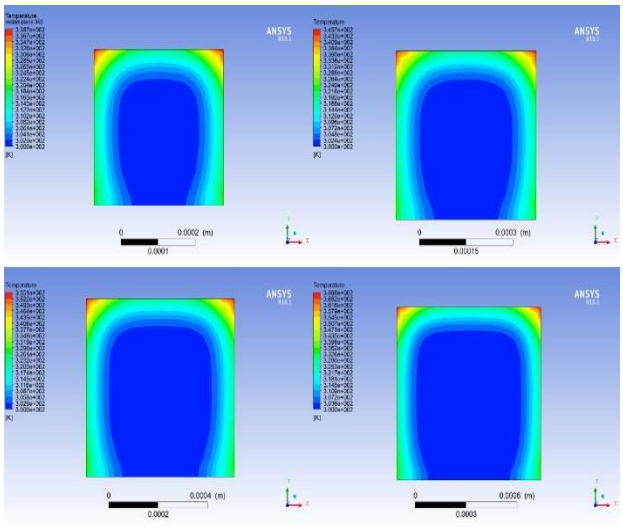

Figure 5. Local temperature on middle plane of microchannels with (AR=1, Dh = 350, 450, 600, 850 µm, Re =800)

3.2. Temperature Distribution and Thermal Boundary Layer

Figure 6 shows the temperature contours along the microchannel length for different Reynolds numbers under constant wall heat flux conditions. At lower Reynolds numbers, higher wall and bulk fluid temperatures are observed due to reduced convective transport and thicker thermal boundary layers. Increasing Reynolds number enhances axial heat convection, leading to lower wall temperatures and a more uniform temperature distribution along the channel.

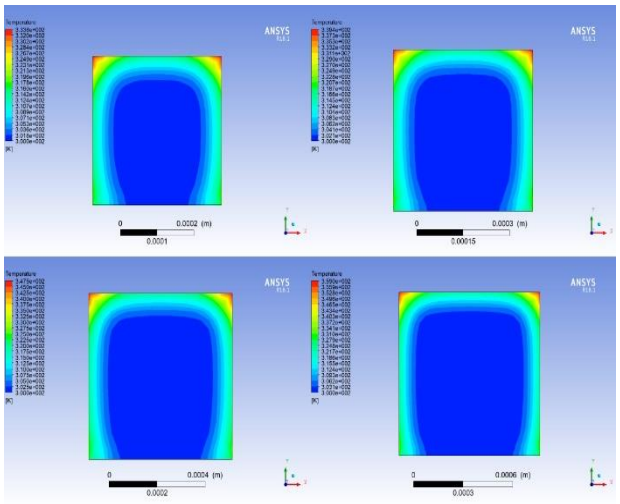

Figure 6. Local temperature on middle plane of microchannels with (AR=1, Dh = 350, 450, 600, 850 µm, Re =1200)

The effect of hydraulic diameter on temperature distribution is presented in Figure 7. Smaller hydraulic diameters result in lower wall temperatures due to the increased surface-area-to-volume ratio, which enhances heat transfer between the heated walls and the nanofluid. In contrast, larger hydraulic diameters exhibit higher wall temperatures, indicating reduced heat removal capability.

Aspect ratio effects on thermal behavior are depicted in Figure 7. Increasing aspect ratio alters the shape of the thermal boundary layer, particularly near the longer walls. However, the results indicate that increasing aspect ratio alone does not guarantee improved thermal performance, as the enhancement depends on the balance between heat transfer area and local flow acceleration near the walls.

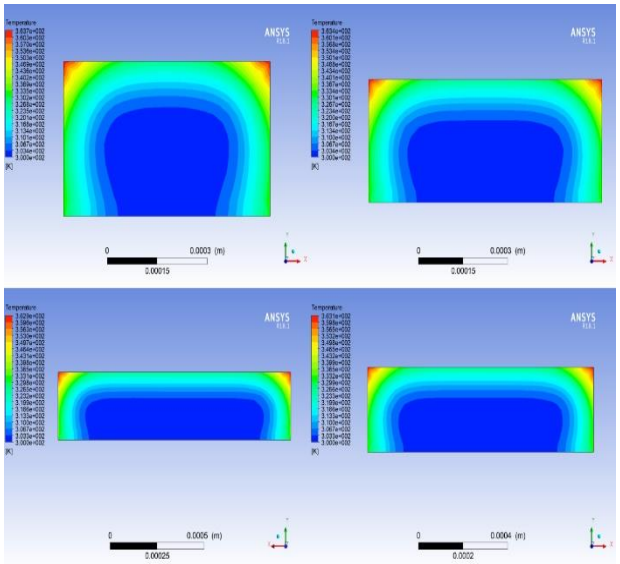

Figure 7. Local temperature on middle plane of microchannels with (Dh = 350, AR =1.75,2.5,3.5,4.5, µm, Re =300)

3.3. Nusselt Number Variation

The variation of the average Nusselt number with Reynolds number for different hydraulic diameters is shown in Figure 8. The Nusselt number increases monotonically with Reynolds number for all cases, confirming that enhanced convective transport dominates heat transfer behavior in the laminar regime. This trend is consistent with classical laminar convection theory and previous microchannel studies.

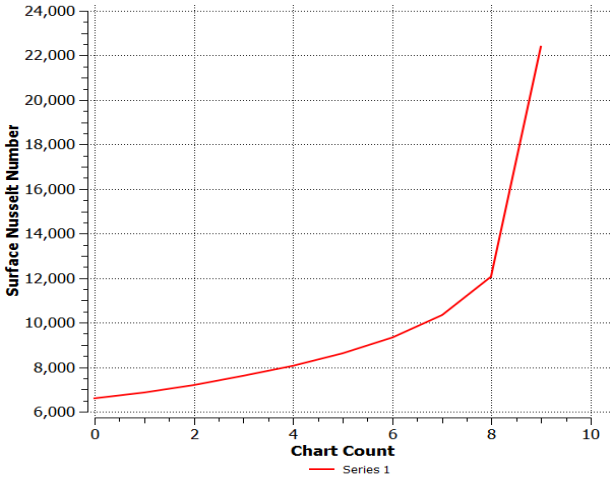

Figure 8. Surface Nusselt number distribution on wall 2 at (AR =1, Dh=350 µm Re=300)

Figure 9 compares the average Nusselt number for different aspect ratios at fixed Reynolds numbers. While moderate increases in aspect ratio lead to slight enhancement in Nusselt number, further increases result in diminishing returns. This behavior can be attributed to non-uniform velocity distribution and localized thickening of the thermal boundary layer in high-aspect-ratio channels.

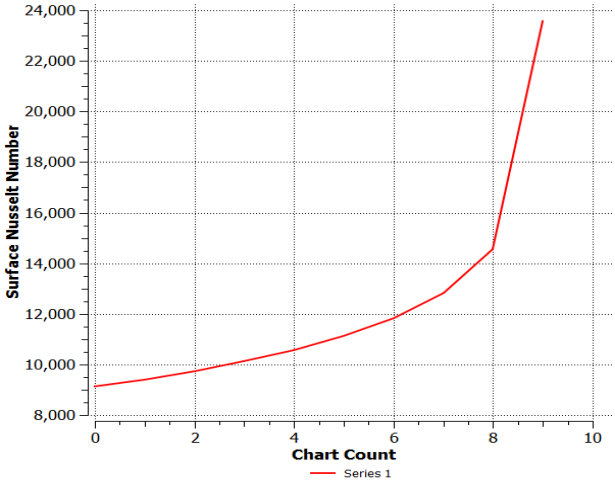

Figure 9. Surface Nusselt number distribution on wall 2 at (AR =1, Dh=350 µm Re=800)

The combined influence of Reynolds number and geometry on heat transfer performance highlights the importance of simultaneous optimization rather than relying on a single geometric parameter.

3.4. Extended planes contours temperature

At Renolds number (Re =300,800, and1200) and aspect ratio (AR=1) as shown in Figures (10, 11, 12, 13, 14, 15, 16, 17, 18 and 19) represent locale temperature profile for three extended planes (upper plane near to the upper wall, middle plane, and bottom plane near to bottom plane). the results show that temperature increases in the direction of microchannel length. The maximum amount of temperature at the outlet especially at the wall's boundary. As before the temperature increases when the hydraulic diameter increases and the upper wall on (Dh =850 µm) has the maximum value of temperature. And The temperature values on the middle plane are less than upper and bottom planes. The results also show that Renolds effect on temperature by increasing it the temperature decrease in different hydraulic dimeters.

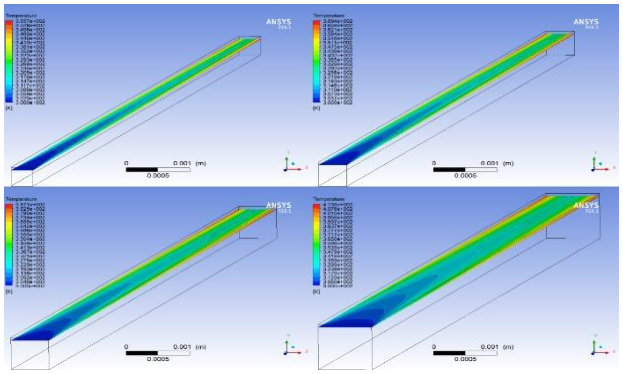

Figure 10. local temperature on extended upper planes of microchannels with (AR=1, Dh = 350, 450, 600, 850 µm, Re =300)

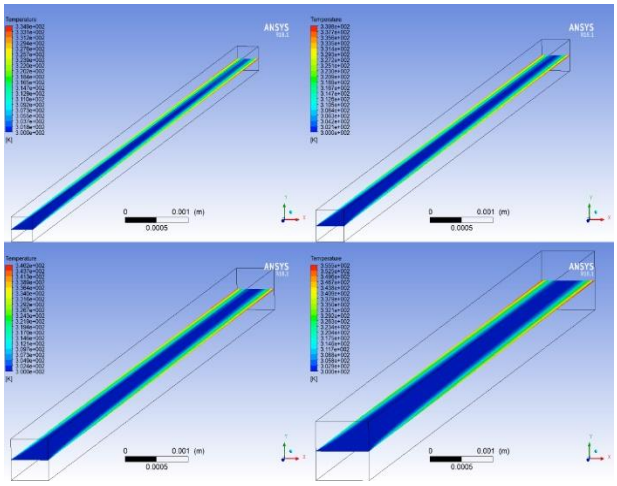

Figure 1. Local temperature on extended middle planes of microchannels with (AR=1, Dh = 250, 450, 600, 850 µm, Re =300)

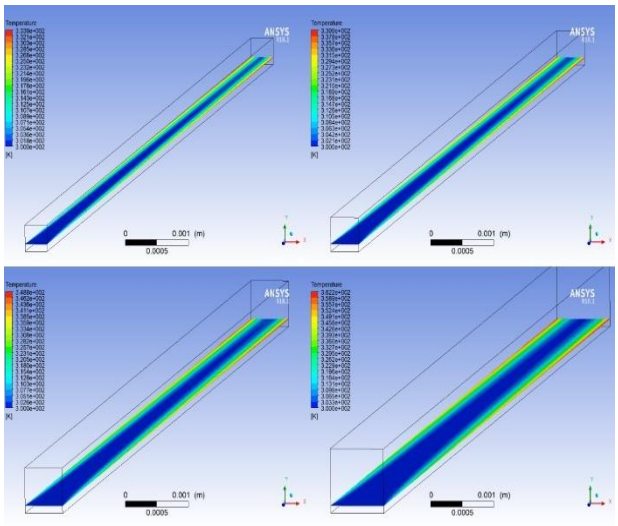

Figure 12. Local temperature on extended bottom planes of microchannels with (AR=1, Dh = 350, 450, 600, 850 µm, Re =300)

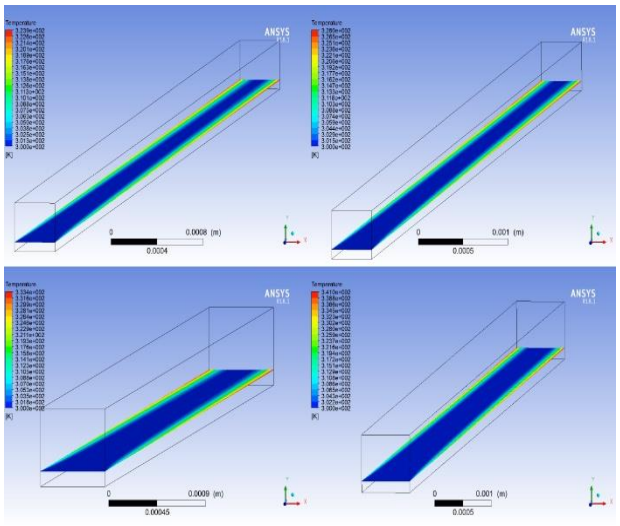

Figure 15. Local temperature on extended bottom planes of microchannels with (AR=1, Dh = 350, 450, 600, 850 µm, Re =800)

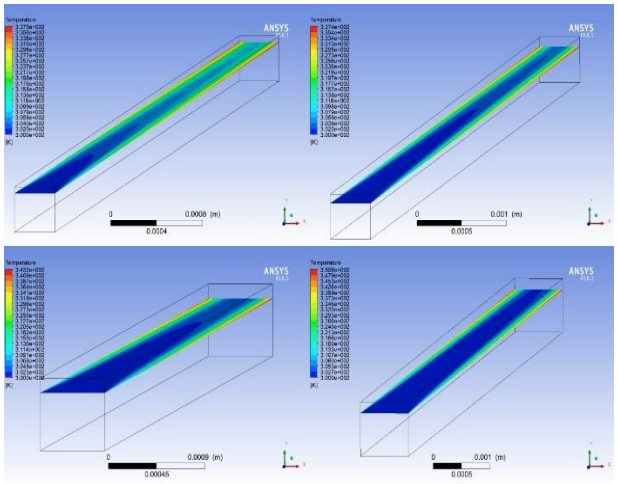

Figure 13. Local temperature on extended upper planes of microchannels with (AR=1, Dh = 350, 450, 600, 850 µm, Re =800)

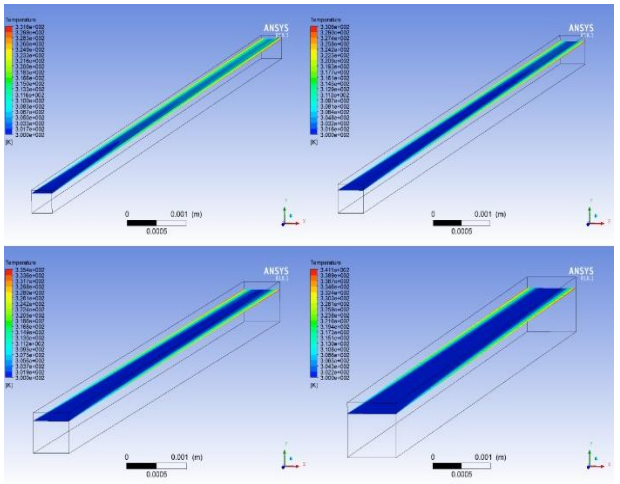

Figure 16. Local temperature on extended upper planes of microchannels with (AR=1, Dh = 350, 450, 600, 850 µm, Re =1200)

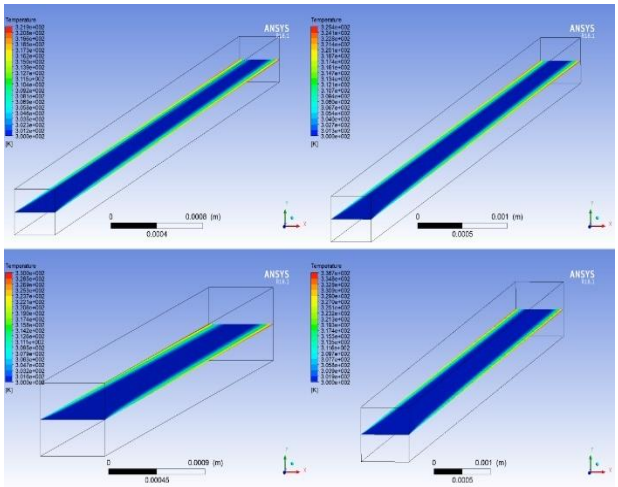

Figure 15. Local temperature on extended middle planes of microchannels with (AR=1, Dh = 350, 450, 600, 850 µm, Re =800)

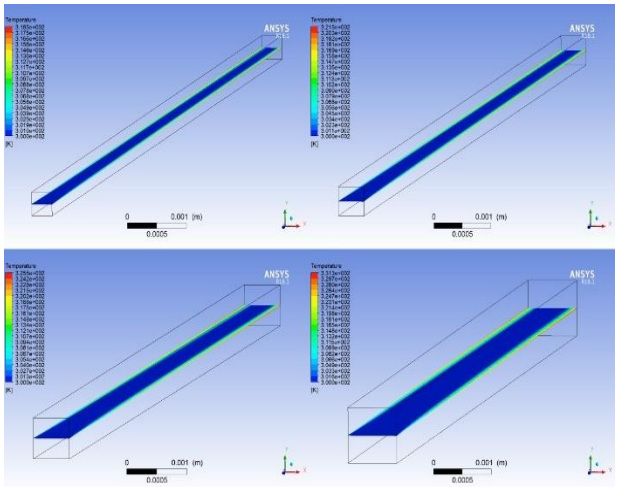

Figure 18. Local temperature on extended middle planes of microchannels with (AR=1, Dh = 350, 450, 600, 850 µm, Re =1200)

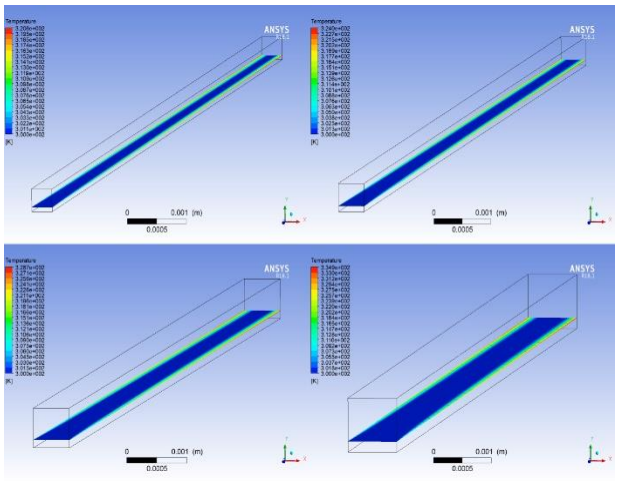

Figure 19. Local temperature on extended bottom planes of microchannels with (AR=1, Dh = 350, 450, 600, 850 µm, Re =1200)

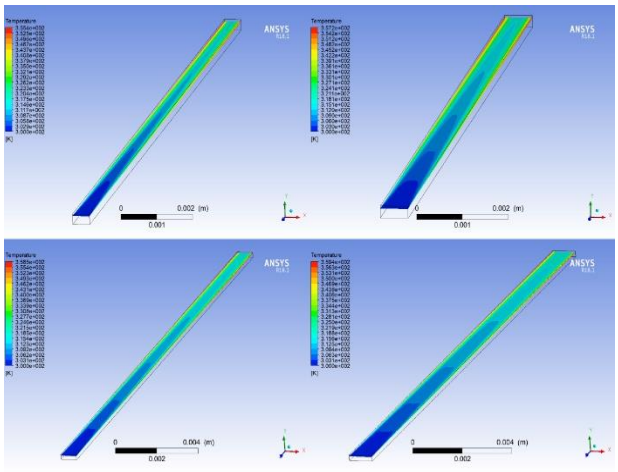

Figure 20. Local temperature on extended upper plane of microchannels with (Dh = 350, AR =1.75,2.5,3.5,4.5, µm, Re =300)

3.5. Thermal–Hydraulic Performance

To evaluate the overall effectiveness of the microchannel configurations, Figure 20 presents Local temperature on extended upper plane of microchannels with (Dh = 450). The results demonstrate that configurations with moderate hydraulic diameters and aspect ratios provide the most favorable balance between heat transfer improvement and pumping power requirements.

Although smaller hydraulic diameters yield higher Nusselt numbers, their significantly higher pressure drops reduce their overall performance. Similarly, very high aspect ratios offer limited thermal benefits while imposing additional hydraulic losses.

In the second method, each hydraulic diameter remains constant and changes in aspect ratios (AR 1.75,2.5,3.5,4.5) and different Reynolds numbers. By taking an extended upper plane near to upper wall the result also shows that temperature increases in the direction of microchannel length. The maximum amount of temperature at the outlet especially at the wall's boundary increases at a small amount with increasing in aspect ratio for each hydraulic diameter. Increasing the hydraulic dimeter has a big effect on temperature values as it increases the temperature also increases. However, the relation between Renold's number and temperature is reversed for all cases. Figures (20-29) show the extended upper plane local temperature contour.

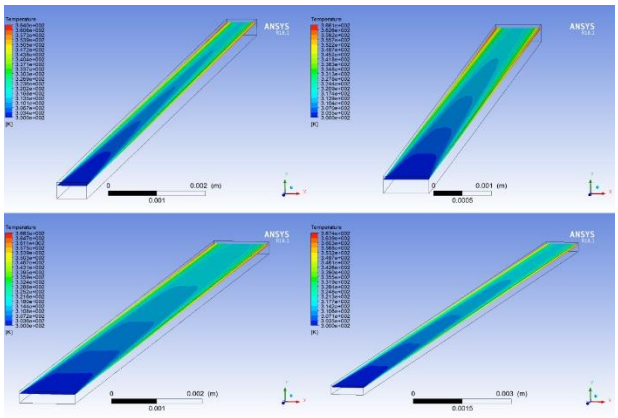

Figure 20. Local temperature on extended upper plane of microchannels with (Dh = 450, AR =1.75,2.5,3.5,4.5, µm, Re =300)

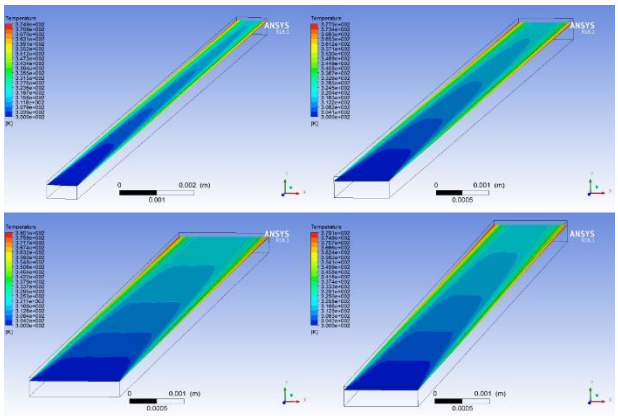

Figure 21. Local temperature on extended upper plane of microchannels with (Dh = 600, AR =1.75,2.5,3.5,4.5, µm, Re =300)

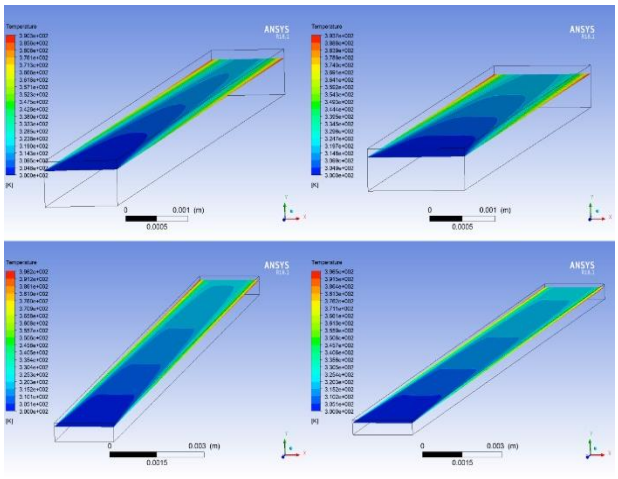

Figure 22. Local temperature on extended upper plane of microchannels with (Dh = 850, AR =1.75,2.5,3.5,4.5, µm, Re =300)

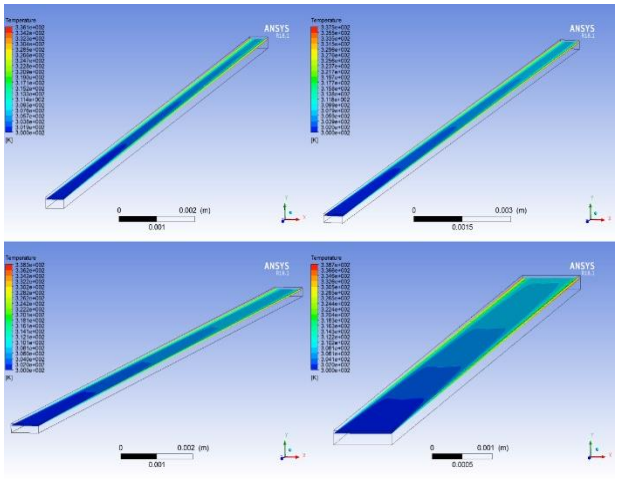

Figure 23. Local temperature on extended upper plane of microchannels with (Dh = 350, AR =1.75,2.5,3.5,4.5, µm, Re =800)

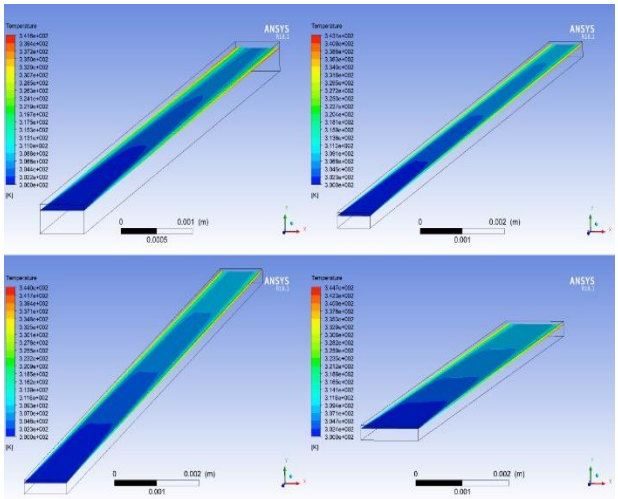

Figure 24. Local temperature on extended upper plane of microchannels with (Dh = 450, AR =1.75,2.5,3.5,4.5, µm, Re =800)

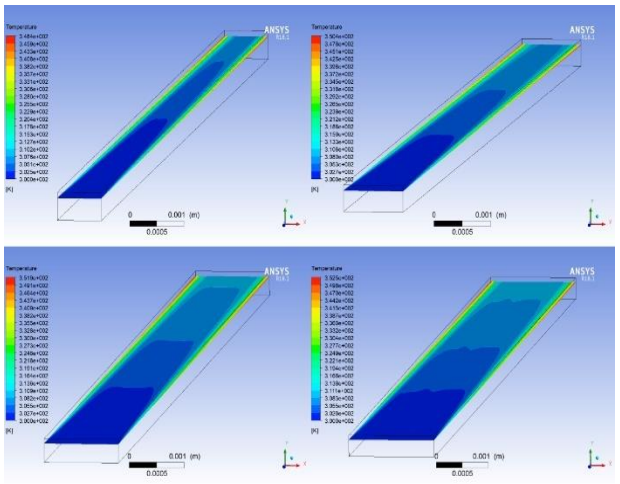

Figure 25. Local temperature on extended upper plane of microchannels with (Dh = 600, AR =1.75,2.5,3.5,4.5, µm, Re =800)

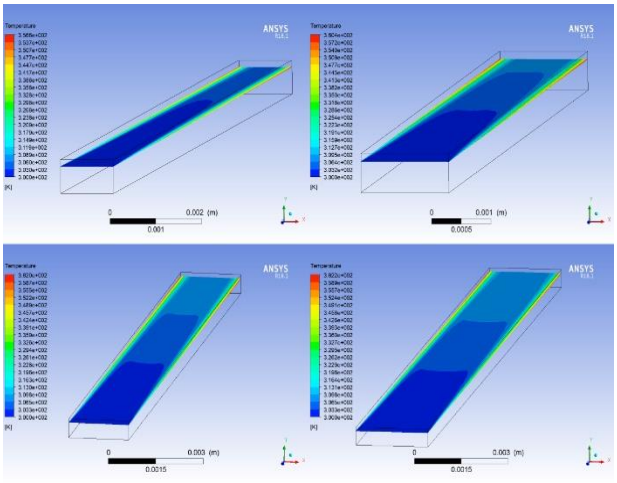

Figure 26. Local temperature on extended upper plane of microchannels with (Dh = 850, AR =1.75,2.5,3.5,4.5, µm, Re =800)

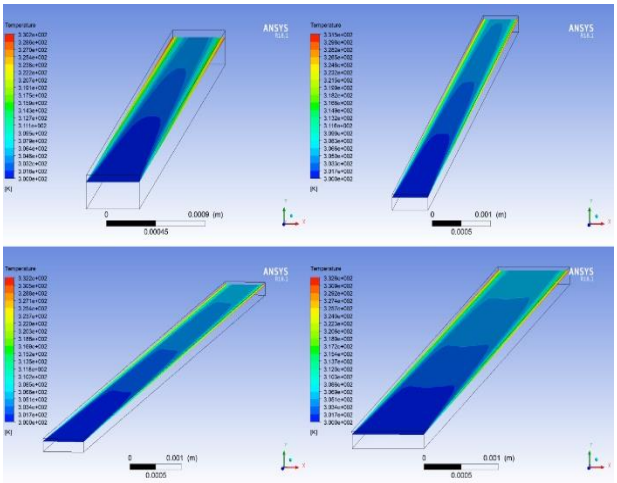

Figure 27. Local temperature on extended upper plane of microchannels with (Dh = 350, AR =1.75,2.5,3.5,4.5, µm, Re =1200)

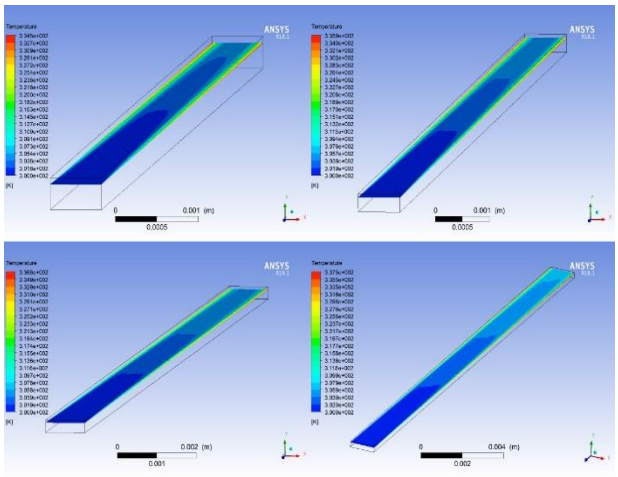

Figure 28. Local temperature on extended upper plane of microchannels with (Dh = 450, AR =1.75,2.5,3.5,4.5, µm, Re =1200)

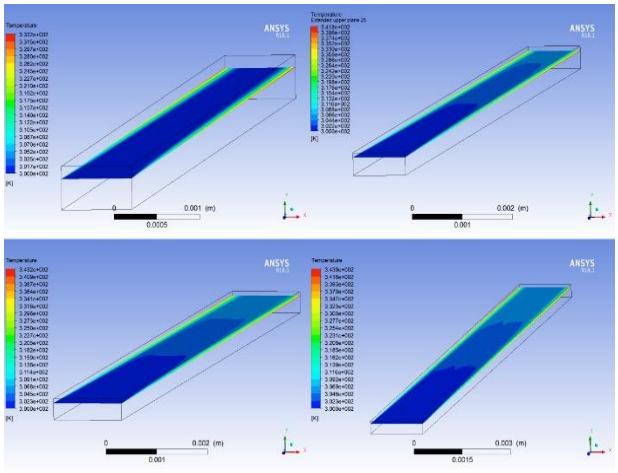

Figure 29. Local temperature on extended upper plane of microchannels with (Dh = 600, AR =1.75,2.5,3.5,4.5, µm, Re =1200)

3.6. Discussion Summary

Overall, the results demonstrate that Reynolds number is the dominant parameter influencing convective heat transfer enhancement in laminar nanofluid flow through rectangular microchannels. Hydraulic diameter strongly affects both heat transfer and pressure drop, while aspect ratio plays a secondary but non-negligible role. The findings emphasize that optimal microchannel performance can only be achieved through a coupled consideration of thermal and hydraulic characteristics rather than isolated parameter selection.

IV. Conclusion

This study presented a comprehensive three-dimensional numerical investigation of laminar nanofluid flow and heat transfer in rectangular microchannels subjected to uniform wall heat flux conditions. The analysis focused on evaluating the coupled effects of Reynolds number, hydraulic diameter, and aspect ratio on flow behavior, thermal performance, and pressure drop characteristics. By systematically examining these parameters, the present work provides useful insight into the fundamental thermal–hydraulic mechanisms governing nanofluid-based microchannel cooling and offers guidance for optimized microchannel heat sink design.

The main findings of this study can be summarized as follows:

- Reynolds number was identified as the dominant parameter governing convective heat transfer enhancement, with increasing Reynolds number significantly improving the average Nusselt number due to thinning of the thermal boundary layer and enhanced axial convection.
- Hydraulic diameter exerted a strong influence on both thermal and hydraulic performance, where smaller hydraulic diameters enhanced heat transfer because of increased surface-area-to-volume ratio but resulted in substantially higher pressure drop.
- Aspect ratio affected velocity redistribution and thermal boundary layer development, particularly near the longer channel walls; however, increasing aspect ratio alone did not guarantee improved heat transfer under laminar flow conditions.
- A clear thermal–hydraulic trade-off was observed, indicating that configurations yielding the highest Nusselt numbers were not necessarily optimal when pressure drop penalties were considered.
- Optimal performance was achieved for moderate values of hydraulic diameter and aspect ratio, where heat transfer enhancement and pumping power requirements were balanced effectively.

The findings of this study provide quantitative design guidance for the development of efficient rectangular microchannel heat sinks using nanofluids in advanced electronic cooling and thermal energy management applications.

Declaration

- The authors declare that they have no known financial or non-financial competing interests in any material discussed in this paper.
- The authors declare that this article has not been published before and is not in the process of being published in any other journal.
- The authors confirmed that the paper was free of plagiarism

References

[1] D. B. Tuckerman and R. F. W. Pease, "High-performance heat sinking for VLSI," IEEE Electron Device Lett., vol. 2, no. 5, pp. 126–129, 1981.

[2] P. Wu and W. A. Little, "Measurement of heat transfer characteristics of gas flow in fine channels," Cryogenics, vol. 24, no. 8, pp. 415–420, 1984, doi: 10.1016/0011-2275(84)90042-7.

[3] S. B. Choi, "Fluid flow and heat transfer in microtubes," ASME Fluids Eng. Div., 1991.

[4] M. M. Rahman and F. Gui, "Experimental investigation of heat transfer in microchannels," in Proc. ASME Electron. Packag. Conf., 1993, pp. 685–692.

[5] M. M. Rahman and F. Gui, "Thermal performance of microchannel heat sinks," in Proc. Intersoc. Energy Convers. Eng. Conf., 1993.

[6] X. F. Peng, G. P. Peterson, and B. X. Wang, "Heat transfer characteristics of water flowing through microchannels," Exp. Heat Transfer, vol. 7, no. 4, pp. 265–283, 1994, doi: 10.1080/08916159408946493.

[7] D. Yu, "Single-phase convective heat transfer in microchannels," in Proc. ASME/JSME Thermal Eng. Conf., 1995, pp. 523–530.

[8] X. F. Peng and G. P. Peterson, "Convective heat transfer and flow friction for water flow in microchannel structures," Int. J. Heat Mass Transfer, vol. 39, no. 12, pp. 2599–2608, 1996, doi: 10.1016/0017-9310(95)00273-5.

[9] T. M. Adams, S. I. Abdel-Khalik, S. M. Jeter, and Z. H. Qureshi, "An experimental investigation of single-phase forced convection in microchannels," Int. J. Heat Mass Transfer, vol. 41, no. 6–7, pp. 851–857, 1998, doi: 10.1016/S0017-9310(97)00122-9.

[10] G. P. Celata, M. Cumo, V. Marconi, and G. Zummo, "Single-phase heat transfer and fluid flow in microtubes," Microscale Thermophys. Eng., vol. 6, no. 2, pp. 85–97, 2002, doi: 10.1080/10893950290054121.

[11] H. Y. Wu and P. Cheng, "An experimental study of convective heat transfer in silicon microchannels," Int. J. Heat Mass Transfer, vol. 46, no. 14, pp. 2547–2556, 2003, doi: 10.1016/S0017-9310(03)00033-1.

[12] A. Bucci, G. P. Celata, M. Cumo, and V. Marconi, "Experimental investigation of fluid flow and heat transfer in microchannels," in Proc. Int. Conf. Nanochannels, Microchannels, Minichannels, 2003.

[13] W. Owhaib and B. Palm, "Experimental investigation of single-phase convective heat transfer in circular microchannels," Exp. Therm. Fluid Sci., vol. 28, no. 2–3, pp. 105–110, 2004, doi: 10.1016/S0894-1777(03)00052-6.

[14] P.-S. Lee, S. V. Garimella, and D. Liu, "Investigation of heat transfer in rectangular microchannels," Int. J. Heat Mass Transfer, vol. 48, no. 9, pp. 1688–1704, 2005, doi: 10.1016/j.ijheatmasstransfer.2004.10.019.

[15] R. Bavière, F. Ayela, and M. Favre-Marinet, "Experimental study of heat transfer and pressure drop in microchannels," Int. J. Heat Mass Transfer, vol. 49, no. 17–18, pp. 3325–3337, 2006, doi: 10.1016/j.ijheatmasstransfer.2006.01.018.

[16] C. Wang, X. F. Peng, and G. P. Peterson, "Convective heat transfer characteristics in microchannels," Sens. Actuators A, vol. 133, no. 2, pp. 323–328, 2007, doi: 10.1016/j.sna.2006.03.020.

[17] J.-Y. Jung, H.-S. Oh, and H.-Y. Kwak, "Forced convection heat transfer in microchannels with rough surfaces," Int. J. Heat Mass Transfer, vol. 52, no. 1–2, pp. 466–472, 2009, doi: 10.1016/j.ijheatmasstransfer.2008.06.025.

[18] O. B. Ergu, O. N. Sara, and S. Yapici, "Experimental investigation of liquid flow in microchannels," Int. Commun. Heat Mass Transfer, vol. 36, no. 6, pp. 618–623, 2009, doi: 10.1016/j.icheatmasstransfer.2009.03.007.

[19] Y.-T. Yang and F.-H. Lai, "Numerical study of heat transfer enhancement in microchannels," Int. J. Heat Mass Transfer, vol. 53, no. 25–26, pp. 5895–5904, 2010, doi: 10.1016/j.ijheatmasstransfer.2010.07.025.

[20] T. Harirchian and S. V. Garimella, "Heat transfer and flow regimes in microchannels," Int. J. Heat Mass Transfer, vol. 51, no. 15–16, pp. 3724–3735, 2008, doi: 10.1016/j.ijheatmasstransfer.2007.12.021.

[21] H. S. Park and J. Punch, "Heat transfer characteristics of water flow in microchannels," Int. J. Heat Mass Transfer, vol. 51, no. 17–18, pp. 4535–4543, 2008, doi: 10.1016/j.ijheatmasstransfer.2007.12.006.

[22] X. Quan, P. Cheng, and J. Li, "Experimental investigation of heat transfer in microchannels," Int. J. Heat Mass Transfer, vol. 53, no. 17–18, pp. 3670–3676, 2010.

[23] S. Prakash and S. Kumar, "Single-phase heat transfer characteristics in microchannels," Proc. IMechE, Part B, vol. 229, no. 7, pp. 1273–1288, 2015, doi: 10.1177/0954405414562386.

[24] N. A. A. Qasem and S. M. Zubair, "Thermal and hydraulic performance of microchannel heat sinks," Energy Convers. Manage., vol. 173, pp. 555–601, 2018, doi: 10.1016/j.enconman.2018.07.084.

[25] H. A. Nabwey et al., "Thermal performance of nanofluids in microchannels," Nanomaterials, vol. 13, no. 5, 2023, doi: 10.3390/nano13050788.

[26] Q. Gravndyan et al., "Thermophysical properties of nanofluids," J. Mol. Liq., vol. 236, pp. 254–265, 2017, doi: 10.1016/j.molliq.2017.04.030.

[27] S. Etaig et al., "Numerical investigation of heat transfer enhancement techniques," Procedia Eng., vol. 157, pp. 404–413, 2016, doi: 10.1016/j.proeng.2016.08.389.

[28] S. Etaig et al., "CFD analysis of microscale heat transfer," Int. J. Numer. Methods Heat Fluid Flow, vol. 28, no. 3, pp. 571–583, 2018, doi: 10.1108/HFF-02-2017-0084.

[29] S. Etaig et al., "Heat transfer enhancement using nanofluids," Int. J. Eng. Res. Technol., vol. 8, no. 12, 2019.

[30] S. Etaig et al., "Nanofluid flow and heat transfer analysis," Amer. J. Nano Res. Appl., vol. 5, no. 4, pp. 102–109, 2017.

[31] S. Etaig et al., "Advanced heat transfer modeling in microchannels," in Proc. CHT-17 ICHMT Symp., 2017.

[32] S. Etaig, Numerical Modeling of Microscale Heat Transfer, Ph.D. dissertation, PQDT-UK & Ireland, 2017.

[33] S. Etaig and G. Hashem, "Numerical investigation of heat transfer enhancement," Int. J. Eng. Res., vol. 1, pp. 1–13, 2022.
[34] S. Etaig and G. Hashem, "CFD analysis of thermal systems," Int. J. Sci. Res., vol. 9, pp. 1588–1592, 2020.
[35] K. S. Hamoudah and S. Etaig, "Numerical investigation of PV/T system cooling using nanofluids," Afr. J. Adv. Pure Appl. Sci., pp. 543–554, 2024.
[36] E. Elabeedy et al., "Performance enhancement of solar energy systems," Solar Energy Sustain. Dev., vol. 14, pp. 17–35, 2025.
[37] K. Hamoudah et al., "Experimental study of thermal systems," in Proc. Sebha Univ. Conf., vol. 3, pp. 252–258, 2024.
[38] D. B. Ingham and I. I. Pop, Transport Phenomena in Porous Media. Oxford, U.K.: Pergamon, 1998.
[39] F. P. Incropera, D. P. DeWitt, T. L. Bergman, and A. S. Lavine, Fundamentals of Heat and Mass Transfer, 6th ed. Hoboken, NJ, USA: Wiley, 1996.
[40] M. Datta et al., "Electrochemical and thermal transport phenomena," ECS Trans., vol. 6, no. 8, pp. 13–31, 2007, doi: 10.1149/1.2744601.
[41] W. Qu, G. M. Mala, and D. Li, "Heat transfer for water flow in trapezoidal silicon microchannels," Int. J. Heat Mass Transfer, vol. 43, no. 21, pp. 3925–3936, 2000, doi: 10.1016/S0017-9310(00)00033-4.
[42] A. Agarwal et al., "Heat transfer and pressure drop in microchannels," Int. J. Refrig., vol. 33, no. 6, pp. 1169–1179, 2010, doi: 10.1016/j.ijrefrig.2010.03.012.
[43] X. F. Peng, G. P. Peterson, and B. X. Wang, "Heat transfer characteristics of water flowing through microchannels," Exp. Heat Transfer, vol. 7, pp. 265–283, 1994, doi: 10.1080/08916159408946493.
[44] P.-S. Lee, S. V. Garimella, and D. Liu, "Investigation of heat transfer in rectangular microchannels," Int. J. Heat Mass Transfer, vol. 48, pp. 1688–1704, 2005, doi: 10.1016/j.ijheatmasstransfer.2004.10.019.
[45] W. Qu, G. M. Mala, and D. Li, "Experimental and numerical study of heat transfer in microchannels," Int. J. Heat Mass Transfer, vol. 43, pp. 3925–3936, 2000, doi: 10.1016/S0017-9310(00)00033-4.